Mon. Not. R. Astron. Soc. **360,** 194–202 (2005) doi:10.1111/j.1365-2966.2005.09028.x

Gravitational collapse in an expanding background and the role of substructure – I. Planar collapse

J. S. Bagla,★ Jayanti Prasad★ and Suryadeep Ray★
Harish-Chandra Research Institute, Chhatnag Road, Jhusi, Allahabad 211019, India

Accepted 2005 March 16. Received 2005 January 21; in original form 2004 August 25

ABSTRACT

We study the interplay of clumping at small scales with the collapse and relaxation of perturbations at much larger scales. We present results of our analysis when the large-scale perturbation is modelled as a plane wave. We find that in the absence of substructure, collapse leads to formation of a pancake with multistream regions. Dynamical relaxation of the plane wave is faster in the presence of substructure. Scattering of substructures and the resulting enhancement of transverse motions of haloes in the multistream region lead to a thinner pancake. In turn, collapse of the plane wave leads to formation of more massive collapsed haloes as compared to the collapse of substructure in the absence of the plane wave. The formation of more massive haloes happens without any increase in the total mass in collapsed haloes. A comparison with the Burgers equation approach in the absence of any substructure suggests that the preferred value of effective viscosity depends primarily on the number of streams in a region.

Key words: gravitation – cosmology: theory – dark matter – large-scale structure of Universe.

1 INTRODUCTION

Large-scale structures like galaxies and clusters of galaxies are believed to have formed by gravitational amplification of small perturbations (Peebles 1980; Peacock 1998; Bernardeau et al. 2002; Padmanabhan 2002). Observations suggest that the initial density perturbations were present at all scales that have been probed by observations. An essential part of the study of formation of galaxies and other large-scale structures is thus the evolution of density perturbations for such initial conditions. Once the amplitude of perturbations at any scale becomes large, i.e. $\delta \sim 1$, the perturbation becomes non-linear and the coupling with perturbations at other scales cannot be ignored. Indeed, understanding the interplay of density perturbations at different scales is essential for developing a full understanding of gravitational collapse in an expanding universe. The basic equations for this have been known for a long time (Peebles 1974) but apart from some special cases, few solutions are known.

A statistical approach to this problem based on the pair conservation equation has yielded interesting results (Hamilton et al. 1991; Nityananda & Padmanabhan 1994; Padmanabhan 1996; Engineer, Kanekar & Padmanabhan 2000), and these results have motivated detailed studies to obtain fitting functions to express the non-linear correlation function or power spectrum in terms of the linearly evolved correlation function (Hamilton et al. 1991; Jain, Mo & White 1995; Peacock & Dodds 1996; Smith et al. 2003).

★E-mail: jasjeet@mri.ernet.in (JSB); jayanti@mri.ernet.in (JP); surya@mri.ernet.in (SR)

It is well known from simulation studies that at the level of second moments, i.e. power spectrum, correlation function, etc., large scales have an important effect on small scales but small scales do not have a significant effect on large scales (Peebles 1985; Little, Weinberg & Park 1991; Klypin & Melott 1992; Bagla & Padmanabhan 1997a; Couchman & Peebles 1998). Most of these studies used the power spectrum as the measure of clustering. Results of these simulation studies form the basis for the use of N-body simulations; e.g. from the above results we can safely assume that small scales not resolved in simulations do not affect power spectrum at large scales and can be ignored.

Substructure can play an important role in the relaxation process. It can induce mixing in phase space (Lynden-Bell 1967; Weinberg 2001), or change halo profiles by introducing transverse motions (Peebles 1990; Subramanian 2000), and gravitational interactions between small clumps can bring in an effective collisionality even for a collisionless fluid (Ma & Bertschinger 2004; Ma & Boylan-Kolchin 2004). Thus it is important to understand the role played by substructure in gravitational collapse and relaxation in the context of an expanding background. In particular, we would like to know if this leaves an imprint on the non-linear evolution of the correlation function. The effect of substructure on collapse and relaxation of larger scales is another manifestation of mode coupling.

In this paper, we report results from a study of mode coupling in gravitational collapse. In particular, we study how the presence of density perturbations at small scales influences collapse and relaxation of perturbations at larger scales. These effects have been studied in the past (Evrard & Crone 1992) but the motivation was slightly different (Peebles 1990). We believe it is important to study the issue in greater detail and make the relevance of these effects

more quantitative using N-body simulations with a larger number of particles. We also study the reverse process, i.e. how does collapse of perturbations at large scales affect density perturbations at much smaller scales.

It is well known that the local geometry of collapse at the time of initial shell crossing is planar in nature (Zel'dovich 1970), hence we model density perturbations as a single plane wave in this work. The simple nature of the large-scale fluctuation allows us to study the interaction of well-separated scales without resorting to statistical estimators like the power spectrum. We are studying the same problem in a more general setting and those results will be reported in a later publication.

The key features of collapse of a plane wave can be understood using quasi-linear approximations, at least at a qualitative level. The initial collapsing phase is well modelled by the Zel'dovich approximation (Zel'dovich 1970), wherein particles fall in towards the centre of the potential well. The Zel'dovich approximation breaks down after orbit-crossing as it does not predict any change in the direction of motion for particles, thus in this approximation particles continue to move in the same direction and the size of the collapsed region grows monotonically. In a realistic situation we expect particles to fall back towards the potential well and oscillate about it with a decreasing amplitude, and the collapsed region remains fairly compact. Several approximations have been suggested to improve upon the Zel'dovich approximation (Gurbatov, Saichev & Shandarin 1989; Shandarin & Zeldovich 1989; Weinberg & Gunn 1990; Matarrese et al. 1992; Brainerd, Scherrer & Villumsen 1993; Bagla & Padmanabhan 1994; Sahni & Coles 1995; Hui & Bertschinger 1996). The adhesion approximation (Gurbatov et al. 1989; Weinberg & Gunn 1990) invokes an effective viscosity: this prevents orbit-crossing and conserves momentum to ensure that the pancakes remain thin and matter ends up in the correct region. This changes the character of motions in dense regions (no orbit-crossing or mixing in the phase space) but predicts locations of these regions correctly. If one assumes that the gravitational potential evolves at a linear rate (Brainerd et al. 1993; Bagla & Padmanabhan 1994), then it can be shown that the collapsed region remains confined. The effective drag due to the expanding background slows down particles and they do not have enough energy to climb out of the potential well.

Thus the process of confining particles to a compact collapsed region results from a combination of expansion of the universe and gravitational interaction of infalling particles. None of the approximations captures all the relevant effects. Therefore we must turn to N-body simulations (Bertschinger 1998; Bagla 2005) in order to study the collapse and relaxation of perturbations in a complete manner.

2 EVOLUTION OF PERTURBATIONS

We will consider only gravitational effects here and ignore all other processes. We assume that the system can be described in the Newtonian limit. The growth of perturbations is then described by the coupled system of Euler's equation and Poisson's equation in comoving coordinates along with mass conservation, e.g. see (Peebles 1980):

$$\begin{aligned} \ddot{\boldsymbol{x}}_i + 2\frac{\dot{a}}{a}\dot{\boldsymbol{x}}_i &= -\frac{1}{a^2}\nabla_i\varphi \\ \nabla^2\varphi = 4\pi G a^2(\rho-\bar{\rho}) &= \frac{3}{2}\frac{\delta}{a^3}H_0^2\Omega_{\rm nr} \\ \rho(\boldsymbol{x}) &= \frac{1}{a^3}\sum_i m_i\delta_{\rm D}(\boldsymbol{x}-\boldsymbol{x}_i). \end{aligned} \tag{1}$$

It is assumed that the density field is generated by a distribution of particles, each of mass m_i, position $\boldsymbol{x}_i$. H_0 is the present value of the Hubble constant, $\Omega_{\rm nr}$ is the present density parameter for non-relativistic matter and a is the scalefactor. In this paper we will consider an Einstein–de Sitter universe as the background, i.e. $\Omega_{\rm nr} = 1$. These can be reduced to a single non-linear differential equation for density contrast (Peebles 1974):

$$\ddot{\delta}_{\boldsymbol{k}} + 2\frac{\dot{a}}{a}\dot{\delta}_{\boldsymbol{k}} = \frac{3}{2}\frac{\delta_{\boldsymbol{k}}}{a^3}H_0^2 + A - B \tag{2}$$

where

$$A = \frac{3}{4}\frac{1}{a^3}H_0^2\sum_{\boldsymbol{k}'\neq 0,\boldsymbol{k}}\left[\frac{\boldsymbol{k}\cdot\boldsymbol{k}'}{k'^2} + \frac{\boldsymbol{k}\cdot(\boldsymbol{k}-\boldsymbol{k}')}{|\boldsymbol{k}-\boldsymbol{k}'|^2}\right]\delta_{\boldsymbol{k}'}\delta_{\boldsymbol{k}-\boldsymbol{k}'} \tag{3}$$

and

$$B = \frac{1}{M}\sum_i m_i\,(\boldsymbol{k}\cdot\dot{\boldsymbol{x}}_i)^2\exp(\mathrm{i}\boldsymbol{k}\cdot\boldsymbol{x}_i)\,; \qquad M = \sum_i m_i. \tag{4}$$

The terms A and B are the non-linear coupling terms between different modes. B couples density contrasts in an indirect manner through velocities of particles ($\dot{\boldsymbol{x}}_i$). The equation of motion still needs to be solved for a complete solution of this equation, or we can use some Ansatz for velocities to make this an independent equation.

It can be shown that individual *virialized* objects, i.e. objects that satisfy the condition $2T + U = 0$ where T is the kinetic energy and U is the potential energy, do not make any contribution towards the growth of perturbations through mode coupling (Peebles 1974) at much larger scales, i.e. the $A - B$ term is zero. The contribution of mode coupling due to the interaction of such objects is not known.

Approximate approaches to structure formation can be developed by ignoring the interaction of well-separated scales. The evolution of density perturbations can be modelled as a combination of non-linear collapse at small scales, and the collapsed objects can be displaced using quasi-linear approximations (Bond & Myers 1996a,b,c; Monaco et al. 2002a; Monaco, Theuns & Taffoni 2002b; Taffoni, Monaco & Theuns 2002). These approaches yield an acceptable description of properties of collapsed objects and their distribution for a first estimate. PINOCCHIO (Monaco et al. 2002a,b; Taffoni et al. 2002) provides sufficient information about halo properties and merger trees for use with semi-analytic models of galaxy formation. The efficacy of these models puts an upper bound on the effects of mode coupling that we are studying here.

In this paper we simplify the system by starting with perturbations that have a non-zero amplitude only for two sets of scales. We simulate the collapse of a plane wave by starting with non-zero amplitude of perturbations for the fundamental mode of the simulation box along the z-axis; the wavenumber of the fundamental mode is denoted by $k_{\rm f}$. This serves as the large-scale perturbation in our study. The amplitude for this mode is chosen so that shell crossing takes place when the scalefactor $a = 1$. The power spectrum for small-scale fluctuations is chosen to be non-zero in a range of wavenumbers $k_0 \pm \delta k$ with a constant amplitude across this window, i.e. $\Delta_s^2(k) = \alpha A$ for $k_0 - \delta k \leqslant k \leqslant k_0 + \delta k$. A Gaussian random realization of this power spectrum is used for small-scale fluctuations. Here $\Delta_s^2(k)$ is the power per logarithmic interval in k contributed by small scales (large k) and A is the amplitude of the fundamental mode that gives rise to the plane wave. The ratio of $\Delta^2(k)$ at $k = k_0$ and for the plane wave is denoted by α, thus when $\alpha = 1$ collapse of perturbations at these scales happens at the same time whereas for $\alpha > 1$ perturbations at small scales collapse before the plane wave collapses. We chose the ratio $k_0/k_{\rm f} = 8$ so that there is a distinct separation in the scales involved.

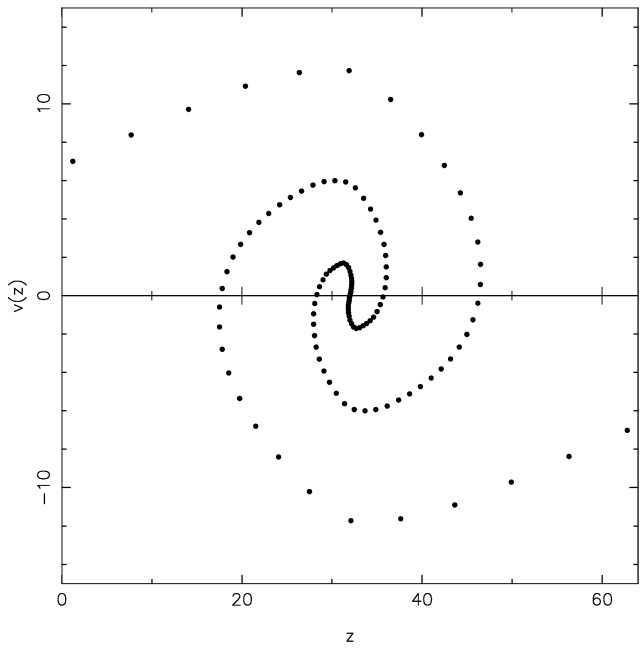

Figure 1. Phase space plot for the plane wave at late stages of collapse for the simulation PM_00L. The velocity of particles is plotted as a function of position. Regions where particles with different velocities can be found are the multistream regions. As we approach the centre of the pancake located at $z = 32$, we go from a single-stream region to a three-stream region and so on up to a seven-stream region near the centre.

Collapse of a plane wave of this kind leads to formation of a multistream region; we will also use the term pancake to describe this region. Fig. 1 shows the phase space plot for the plane wave at late stages of collapse for the simulation PM_00L (see Table 1 for details of the simulation). The velocity of particles is plotted as a function of position; only the z-component is plotted as there is no displacement or velocity along other directions in this simulation. Regions where particles with different velocities can be found are the multistream regions. As we approach the centre of the pancake located at $z = 32$, we go from a single-stream region to a three-stream region and so on up to a seven-stream region near the centre.

In the initial stages, the mass in the pancake increases rapidly as more particles fall in. Fig. 2 shows this in terms of overdensity which increases sharply from $a = 1$ to $a = 2$. A significant fraction of the total mass falls into the pancake and the infall velocities for the remaining matter are very small. In this regime the mass of the pancake is almost constant; this can be seen from the panels of Fig. 8 (later) where the mass enclosed in the pancake region is almost constant from $a = 2$ to $a = 4$.

In the absence of any substructure the collisionless collapse retains planar symmetry and we have layers of multistream regions with the number of streams increasing towards the centre of the pancake. The presence of small-scale fluctuations can induce transverse motions and these motions are amplified in the pancake.

A weakly bound substructure can be torn apart due to interaction with rapidly infalling matter. On the other hand, a higher average density in the multistream region can lead to rapid growth of perturbations. It is known that pancakes are unstable to fragmentation due to growth of perturbations (Valnia et al. 1997). The velocity field is anisotropic due to infall along one direction, hence the rate at which perturbations grow will also exhibit anisotropies.

Table 1. This table lists the parameters of N-body simulations we have used. All the simulations used 128^3 particles. The first column lists the name of the simulation, the second column lists the code that was used for running the simulation, the third column gives the relative amplitude of small-scale power and the plane wave, the fourth column tells us whether the large-scale plane wave was present in the simulation or not, and the last column lists the distribution of particles before these are displaced using a realization of the power spectrum. *Grid* distribution means that particles started from grid points. *Perturbed grid* refers to a distribution where particles are randomly displaced from the grid points; this displacement has a maximum amplitude of 0.05 grid points. Such an initial condition is needed to prevent particles from reaching the same position in plane-wave collapse as such a situation is pathological for tree codes. The TREEPM simulations were run with a force softening length equal to the grid length.

Name	Method	α	Plane wave	IC
PM_00L	PM	0.0	Yes	Grid
T_00L	TREEPM	0.0	Yes	Perturbed grid
T_05L	TREEPM	0.5	Yes	Grid
T_10L	TREEPM	1.0	Yes	Grid
T_20L	TREEPM	2.0	Yes	Grid
T_40L	TREEPM	4.0	Yes	Grid
T_10P	TREEPM	1.0	Yes	Perturbed grid
T_40P	TREEPM	4.0	Yes	Perturbed grid
T_05	TREEPM	0.5	No	Grid
T_10	TREEPM	1.0	No	Grid
T_20	TREEPM	2.0	No	Grid
T_40	TREEPM	4.0	No	Grid

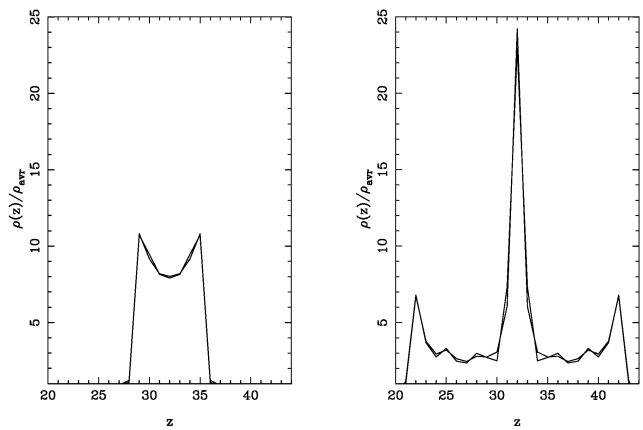

Figure 2. Density profile plotted for two epochs for simulations PM_00L and T_00L. In these simulations density varies only in the direction along the plane wave. Solid lines show the density profile at $a = 1$ and $a = 2$ from the PM_00L simulation; dashed lines show the density profile from the T_00L simulation with the same profile.

Velocity dispersion along the direction of plane wave collapse is larger than the transverse direction, hence the growth of fluctuations in the transverse plane is expected to be more rapid.

If the infalling material contains collapsed substructure, then gravitational interactions between these can induce large transverse velocities. This takes away kinetic energy from the direction of infall, which in turn can lead to a more fragmented and thinner multistream region.

In the following sections we describe the numerical experiments we have undertaken in detail, and test the physical ideas and expectations outlined above.

3 NUMERICAL EXPERIMENTS AND RESULTS

We used a particle-mesh code (Bagla & Padmanabhan 1997b) and the TreePM code (Bagla 2002; Bagla & Ray 2003). Some simulations were run using the parallel TreePM (Ray & Bagla 2004). TreePM simulations used spline softening with softening length equal to the length of a grid cell in order to ensure collisionless evolution. We used force softening assuming a spline kernel (Springel, Yoshida & White 2001). All the simulations were carried out with 128^3 particles. Table 1 lists parameters of the simulations we have used for this paper. We have used two types of initial distribution of particles. In the *Grid* distribution particles are located at grid points before being displaced to set up the initial perturbations. *Perturbed grid* refers to a distribution where particles are randomly displaced from the grid points (Bagla & Padmanabhan 1997b); this displacement has a maximum amplitude of 0.05 grid length. Such an initial condition is needed to prevent particles from reaching the same position in plane-wave collapse as such a situation is pathological for tree codes. These small displacements do not affect the power spectrum to be realized; PM_00L and T_00L were compared to test for any systematic effects.

Simulations T_10P and T_40P were similar to T_10L and T_40L except that the small-scale fluctuations were restricted to the direction orthogonal to the direction of the plane wave. Thus the small-scale fluctuations had the same form for all z. These simulations are useful for differentiating between competing explanations for results outlined below.

In addition to the N-body simulations listed in Table 1, we also carried out one dimensional simulations within the adhesion model (Gurbatov et al. 1989) with a finite viscosity following a method similar to the one outlined by Weinberg & Gunn (1990).

Fig. 2 shows the density profile of the pancake for PM_00L and T_00L simulations at two epochs. These figures demonstrate that the density profiles in these simulations are almost identical, indeed the tiny differences can be attributed to the different initial distribution of particles. We have checked this assertion by running the PM_00L with the perturbed grid initial conditions. The TreePM method has a slightly better resolution but it does not induce any new features. This is expected as the force softening length used in the TreePM simulations is one grid length, the same as the average interparticle separation, and it has been shown than such force softening does not induce two-body collisions (Melott et al. 1997; Splinter et al. 1998). We will mostly use TreePM simulations for the remaining part of this study.

3.1 Thickness of the pancake

An important indicator of the role played by substructure is the thickness of the pancake that forms by collapse of the plane wave. If the substructure does not play an important role in the evolution of large-scale perturbations then the thickness of the pancake should not change by a significant amount. On the other hand, if the substructure does indeed speed up the process of dynamical relaxation then we should see some signature in terms of the thickness of the pancake, velocity structure, or both. Any such effect will be apparent only at late times as infall of matter into the pancake dominates at early times. The dynamical effects of substructure will become important only at late times.

Fig. 3 shows a slice from some of the simulations listed in Table 1. The plane wave collapses along the vertical axis. The configuration at $a = 2$ is shown here; the plane wave begins to collapse at $a = 1$. The different panels in this figure refer to simulations T_00L, T_10L and T_40L. The boundary of the multistream region is clearly visible in all the slices even though this region is fragmented in the last panel (T_40L). It is clear that the pancake is thinner in simulations with more substructure.

A more detailed comparison of simulations with a different level of substructure is shown in Fig. 4. The top panel of this figure shows the averaged overdensity as a function of the z-coordinate; the plane wave collapses along this axis. Overdensity is averaged over all x and y for a given interval $(z \pm \Delta z)$ to obtain the averaged values plotted here. The peak overdensity at the centre of the pancake is smaller in simulations with more substructure. The mass enclosed within a given distance of the centre of the pancake (defined here as the trough of the potential well of the plane wave) is smaller for more substructure, even though the variation is very small at less than 10 per cent between the extreme cases (see Fig. 8, later). Potential wells corresponding to substructure prevent infall into the pancake region. As the amount of substructure is increased, there is visible reduction in the size of the region around the pancake where the density is greater than average. The visual impression of Fig. 3 is reinforced by the variation of overdensity.

The middle panel of Fig. 4 shows the rms velocities of particles in a direction transverse to the plane-wave collapse as a function of the z-coordinate. As in the top panel, averaging is done over all x and y for a given interval $(z \pm \Delta z)$. This plot shows that the transverse motions are enhanced in the dense pancake region. The amplitude of transverse motions is larger in simulations with more substructure. The size of the region where these motions are significant varies with

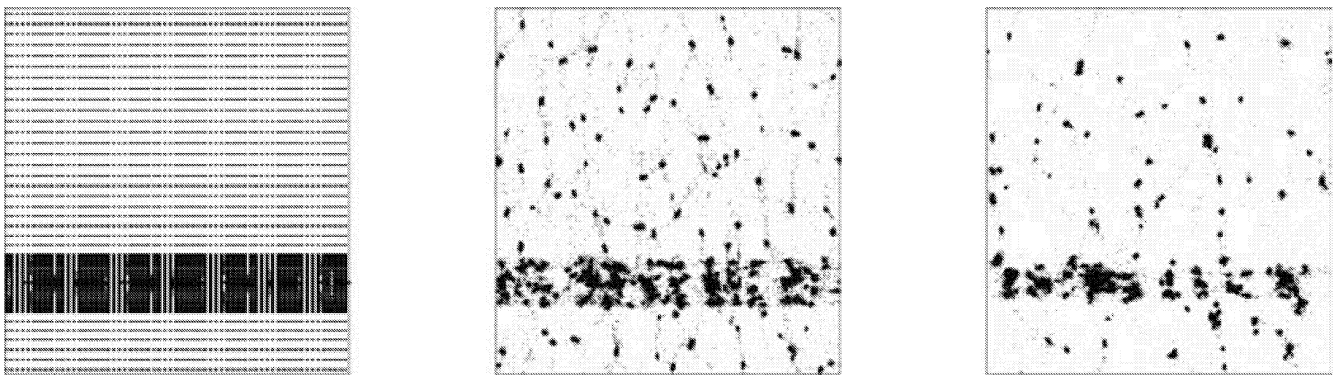

Figure 3. Panels in this figure show the same slice from simulation T_00L, T_10L and T_40L. These slices are shown for $a = 2$, the plane wave begins to collapse at $a = 1$. The plane wave collapses along the vertical direction in these slices. The left panel is for T_00L, the middle panel is for T_10L and the right panel is for T_40L.

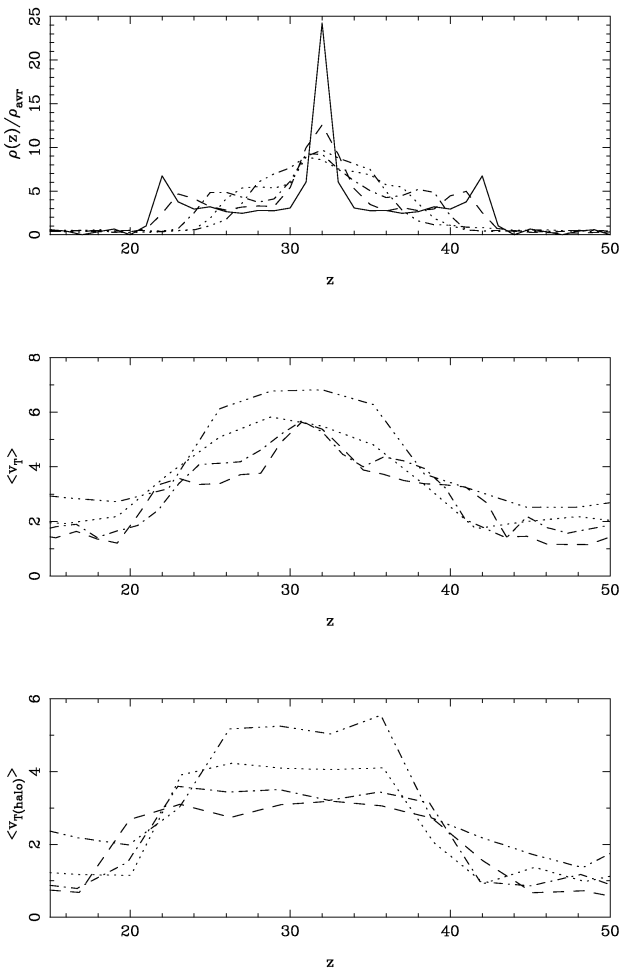

Figure 4. The top panel in this figure shows the density profile as a function of z, the direction of collapse for the plane wave. The density profile has been averaged over the directions transverse to the collapse of the plane wave. The curves are for $a = 2$; simulations used are T_00L (solid line), T_05L (dashed line), T_10L (dot-dashed line), T_20L (dotted line) and T_40L (dot-dot-dashed line). The middle panel shows the rms transverse velocities of particles at the same epoch for T_05L (dashed line), T_10L (dot-dashed line), T_20L (dotted line) and T_40L (dot-dot-dashed line). The lower panel shows the rms transverse velocities of collapsed haloes at the same epoch for T_05L (dashed line), T_10L (dot-dashed line), T_20L (dotted line) and T_40L (dot-dot-dashed line).

the amount of substructure, as in case of overdensity (top panel). The rms transverse velocities do not go to zero outside the pancake region, instead these level off to a small residual value.

Transverse motions are due to motions of particles in clumps that constitute substructure, due to infall of particles in these clumps, and transverse motions of clumps as they move towards each other. In order to delineate these effects, we have plotted the rms velocities for haloes in the last panel of Fig. 4. These haloes were selected with the friends-of-friends (FOF) algorithm using a linking length of $l = 0.2$ grid length. The transverse component of the velocity of centre of mass for haloes with more than 50 particles was used for the figure. Such a high cutoff for halo members is acceptable because typical haloes have several hundred members; see the following subsection on mass functions. Differences between simulations with different amounts of substructure are more pronounced than in the middle panel. For simulations with a small amount of substructure, the motion of clumps is subdominant and hence the transverse motions are contributed mostly by internal motions and infall. In simulations with more substructure, motions of clumps contribute significantly to the rms transverse velocity. The gravitational attraction of clumps, particularly in close encounters in the pancake region, induce the transverse component. Collisions are enhanced in the pancake region as the number density of clumps is higher.

In order to convince ourselves that transverse motions induced by scattering/collision of clumps is the most likely reason for the reduced thickness of pancakes, we compare simulations T_10L and T_40L with T_10P and T_40P. In simulations T_10P and T_40P, the small-scale fluctuations do not have any z-dependence. In these simulations (T_10P and T_40P) there are no clumps but streams of particles that are falling in and this reduces the number of scatterings that take place – no z-dependence means that dense streams run into each other head-on with grazing collisions happening only rarely. Of course, in the simulation the presence of the plane wave leads to breaking of these streams into clumps as the streams are stretched inhomogeneously in the z-direction. These clumps are aligned parallel to the z-axis. In the pancake region scattering of these streams occasionally leads to complex patterns.

If the presence of substructure and its growth in the pancake was the only cause for making the pancake thinner then the pancake in these simulations should be thinner as well. Fig. 5 shows slices from simulations T_40L and T_40P for $a = 2$. A slice from the simulation PM_00L is also plotted here for reference. This visual comparison shows that the pancake is thinner in T_40L as compared to T_40P. Indeed, the thickness of the pancake in T_40P and PM_00L is very

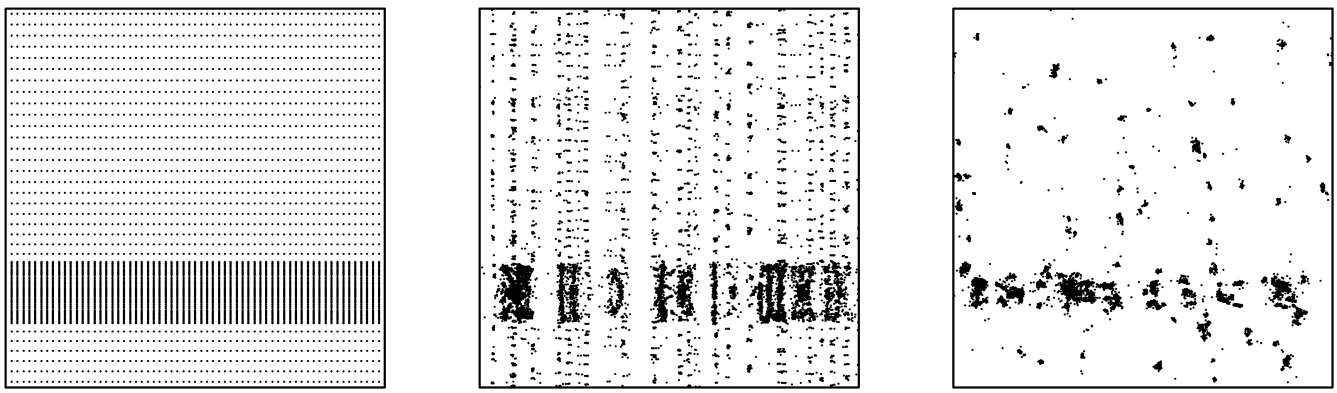

Figure 5. This figure shows slices from simulations T_40L and T_40P for $a = 2$. The left panels shows a slice from the simulation PM_00L, plotted here for reference. The central panel is for T_40P and the right panel is for T_40L. This visual comparison shows that the pancake is thinner in T_40L as compared to T_40P. Indeed, the thickness of the pancake in T_40P and PM_00L is very similar.

similar. This reinforces the point that scattering of clumps in the pancake region is the key reason for thinner pancakes.

Fig. 6 shows the same slice from simulations T_05L, T_05, T_20L and T_20 at three epochs, $a = 0.5$, 1.0 and 2.0. This figure brings out the effect of the plane wave on the collapse of perturbations at small scales as well as the influence of small-scale fluctuations on the thickness of the pancake formed by collapse of the plane wave.

3.2 Pancakes and viscosity

The substructure helps to confine the pancake to a smaller region. It is interesting to study the collapse of a plane wave in an N-body simulation and compare it with the collapse in the adhesion model (Gurbatov, Saichev & Shandarin 1989) with a finite effective viscosity. We first study the collapse of a plane wave in the absence of any substructure (N-body simulation PM_00L) for comparison with numerical simulations of the adhesion model with finite effective viscosity. One-dimensional adhesion simulations were done using the plane wave with the same amplitude as the N-body simulations. We use the standard method for computing the trajectories of particles in the adhesion model (Weinberg & Gunn 1990); a summary of the basic formalism is reproduced here for reference.

In the adhesion approximation, the equation of motion for a particle is replaced by the Burgers equation (Gurbatov Saichev & Shandarin 1989; Weinberg & Gunn 1990). In the one-dimensional situation we are considering here, we have:

$$\frac{\partial u}{\partial b} + u\frac{\partial u}{\partial x} = \nu\frac{\partial^2 u}{\partial x^2}. \tag{5}$$

Here $u = \partial x/\partial b$ is the 'velocity' of particles and b is the linear growth factor. This equation can be solved by introducing the velocity potential $u = \partial\psi/\partial x$, where ψ coincides with the gravitational potential at the initial time. The solution has the following form:

$$u = \nabla\psi = -2\nu\nabla \ln U \tag{6}$$

and

$$U(x,b) = \left(\frac{1}{4\pi\nu b}\right)^{1/2} \int_{-\infty}^{\infty} \exp\left[-\frac{\psi(q)}{2\nu} - \frac{(x-q)^2}{4\nu b}\right] \mathrm{d}q. \tag{7}$$

Here q is the Lagrangian position of the particle and x is the Eulerian position. In this method we integrate the differential equation for particle trajectories. At each time-step, the velocity is calculated by the above procedure at grid points and interpolated to particles positions.

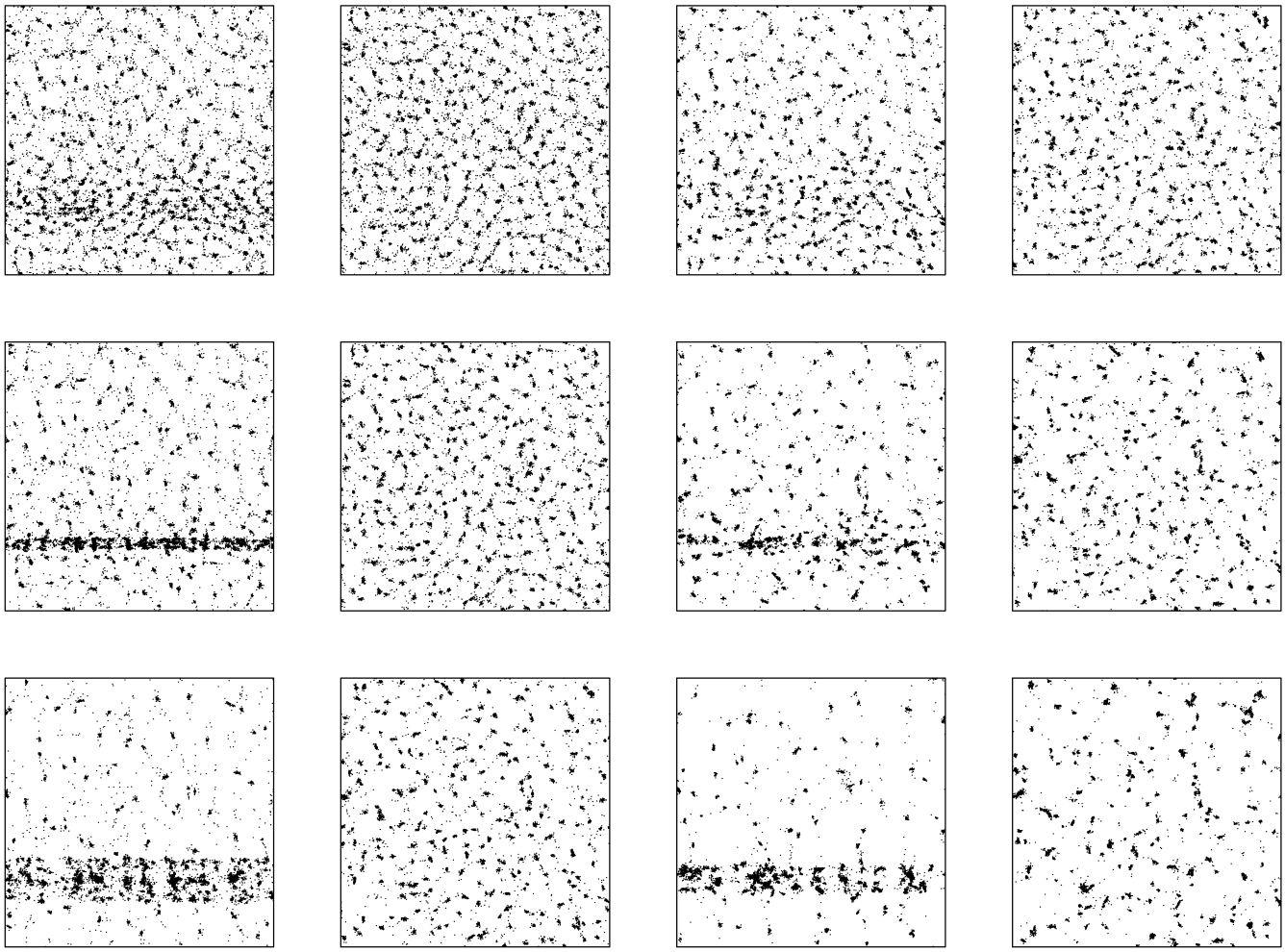

Figure 6. This figure shows the effect of a plane wave on the evolution of small-scale fluctuations. Panels in this figure show a slice from N-body simulations. The top row is for $a = 0.5$, the middle row is for $a = 1$ and the lower row is for $a = 2$. The left column is for T_05L, the second column is for T_05, the third column is for T_20L and the right column is for T_20.

Fig. 7 shows the mass enclosed within a distance z from the centre of the pancake. The enclosed mass is defined as:

$$M(z) = \int_{z_c}^{z_c+z} \mathrm{d}z \rho(z + z_c). \quad (8)$$

Here $\rho(z)$ is the density at position z and z_c is the centre of the pancake. There is no ambiguity for comparing the results with N-body simulations in case of no substructure as the density depends only on z. While comparing other simulations with the adhesion solution, we will consider the density averaged over the x- and y-directions. The adhesion model is run only for the one-dimensional problem. The top panel of Fig. 7 shows the enclosed mass $M(z)$ at $a = 2.0$, middle panel is for $a = 3$ and the lower panel is for $a = 4.0$. The solid curve shows the enclosed mass for PM_00L. In the region with a given number of streams, the N-body curve is smooth. Jumps in mass enclosed occur at the transition from single-stream to multistream regions, and at other transitions where the number of streams changes within the multistream region. All other curves show $M(z)$ for the adhesion model: the dashed curve is for $\nu = 400$, the dotted curve is for $\nu = 600$ and the dot-dashed curve is for $\nu = 900$. There is no constant effective viscosity curve that follows the N-body curve closely through the multistream regions. In regions with a given number of streams, the N-body curve stays around a curve for constant effective viscosity in the adhesion model. A remarkable fact is that the N-body curve for the three-stream region at all the epochs follows the adhesion model curve for $\nu = \simeq 600$. Similar behaviour is seen for the five-stream region which follows $\nu \simeq 900$ though the range of scales and epochs over which this can be resolved is somewhat limited.

Addition of substructure clearly changes the character of the problem and the collapse is no longer one-dimensional. However, the scale of the substructure is so small compared to the wavelength of the plane wave that the large-scale collapse is still very close to planar. Fig. 8 shows the mass enclosed within a distance z from the centre of the multistream region for simulations PM_00L, T_10L and T_40L. The density is averaged over all x and y for this plot in

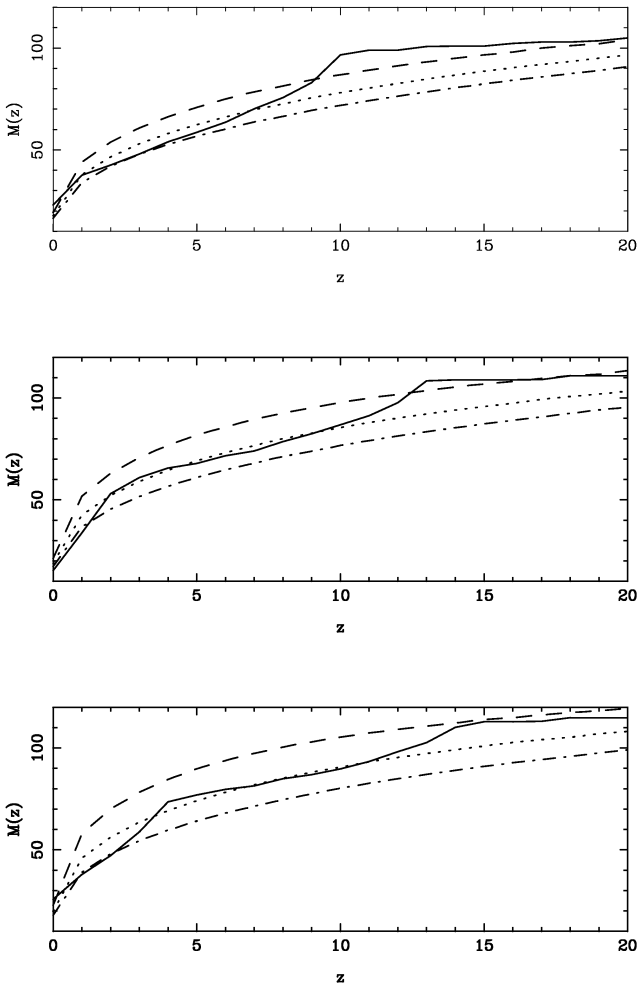

Figure 7. This figure shows the mass enclosed within a distance z from the centre of the multistream region. The top panel shows the curves for $a = 2$. The thick solid curve is for the N-body simulation PM_00L. Jumps in the mass enclosed occur at transition from the multistream region with $2n + 1$ streams to $2n + 3$ streams, with n a non-zero positive integer. All other curves show $M(z)$ for the adhesion model: the dashed curve is for $\nu = 400$, the dotted curve is for $\nu = 600$ and the dot-dashed curve is for $\nu = 900$. The middle panel shows the same set of curves for $a = 3$ and the lower panel is for $a = 4$.

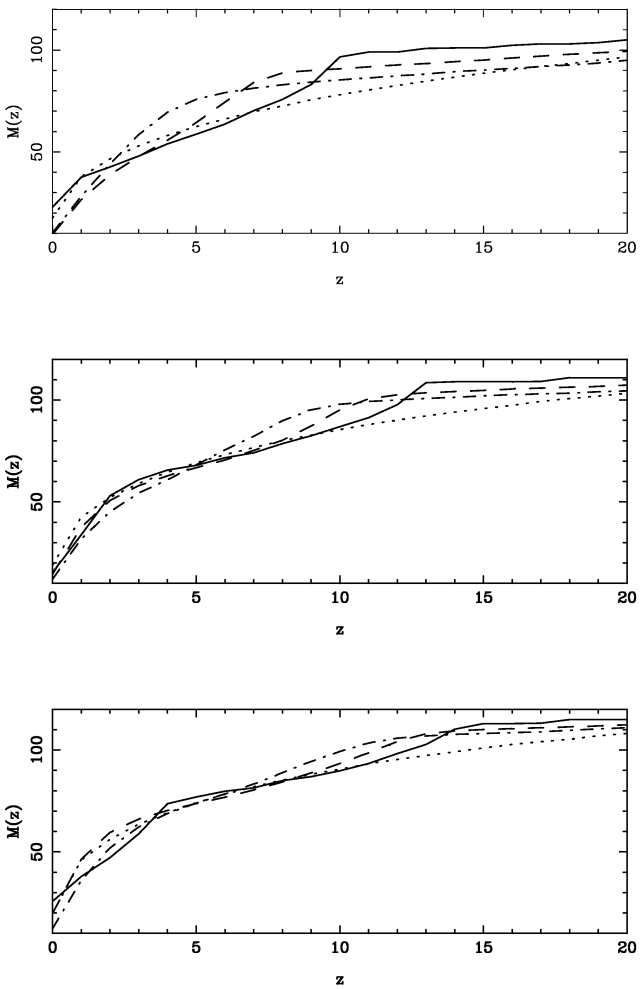

Figure 8. This figure shows the mass enclosed within a distance z from the centre of the multistream region. The top panel shows the curves for $a = 2$. The solid curve is for N-body simulation PM_00L. Other simulations are also plotted here: T_10L (dashed curve) and T_40L (dot-dashed curve). The dotted curve shows the mass enclosed in the one-dimensional adhesion model with $\nu = 600$. The lower panel shows the same set of curves for $a = 4$ and the middle panel is for $a = 3$.

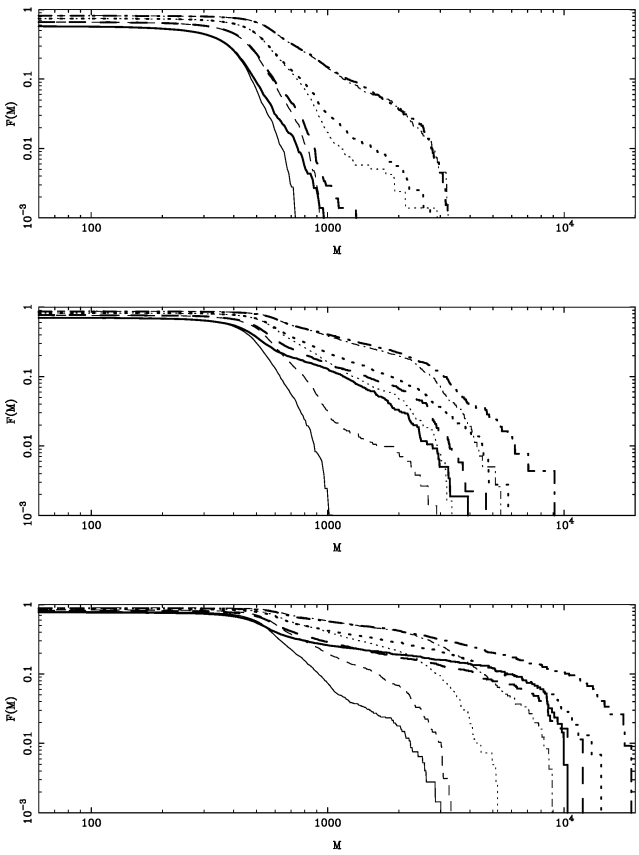

Figure 9. This figure shows the cumulative mass function $F(M)$ as a function of mass M in N-body simulations. The top panel is for $a = 0.5$, the middle panel is for $a = 1$ and the lower panel is for $a = 2$. Curves are shown for T_05 (solid curve), T_05L (thick solid curve), T_10 (dashed curve), T_10L (thick dashed curve), T_20 (dotted curve), T_20L (thick dotted curve), T_40 (dot-dashed curve) and T_40L (thick dot-dashed curve).

the same manner as for Fig. 4. Also plotted in the figure are curves for the adhesion model ($\nu = 600$), where the calculation is done without taking substructure into account. The motivation for such a comparison is to see the effect of substructure on the favoured value of the effective viscosity. The substructure removes the sharp change in density at the boundaries of the three-stream, five-stream and seven-stream regions and the curves for T_10L and T_40L are smoother in the pancake region. The finite viscosity curve matches simulations with substructure over a wider range of scales than with PM_00L. There are no other noteworthy differences.

3.3 Mass function

The mass function of collapsed haloes in these simulations can be used to understand the influence of plane-wave collapse on substructure. Collapsed structures form in these simulations primarily due to initial density fluctuations at small scales, with some modulation by the collapse of the plane wave. In this section we study the effect of the collapsing plane wave on the mass function of collapsed haloes.

These haloes were selected with the friends-of-friends algorithm using a linking length of $l = 0.2$ grid length. The initial power spectrum has a peak at the scale corresponding to 1/8 of the simulation box, or 16 grid lengths. Thus typical haloes will have a Lagrangian radius of about eight grid lengths and should contain about 500 particles. Thus a cutoff of 50 or more particles for haloes is reasonable for this study.

In the absence of the plane wave, the only perturbations are at small scales. The small-scale perturbations are concentrated around a given mass-scale and the mass function is also peaked around this mass at early epochs. At late epochs mergers lead to formation of haloes with a larger mass and the range of masses is greater for models with a larger amplitude of fluctuations. Fig. 6 shows these features in the distribution of particles. These features can also be seen in Fig. 9 where the mass fraction $F(M)$ for $a = 0.5$, 1.0 and 2.0 is plotted in different panels. $F(M)$ is the fraction of total mass in collapsed haloes with halo mass above M.

Adding the plane wave at a much larger scale than the small-scale fluctuations essentially pushes much of the mass into the pancake region, leaving a small fraction of matter in the underdense regions that occupy much of the volume. The growth of small-scale fluctuations in the underdense regions is inhibited whereas growth of fluctuations in the pancake region is enhanced; this is seen clearly in the slices from simulations shown in Fig. 6. Higher background density in the pancake region leads to rapid growth of perturbations; mergers of haloes also lead to formation of massive clumps. These effects become more pronounced at late epochs and result in a shift of mass function towards larger masses; indeed haloes at two distinct mass-scales are present. Low-mass clumps in underdense regions have the mass expected of haloes in regions where small-scale fluctuation dominate, whereas haloes of a much higher mass are present in the pancake region. Fig. 9 shows these two mass-scales very clearly.

The total mass in collapsed haloes does not change significantly with the addition of the plane wave. Indeed for simulations T_40L and T_40, the mass function is the same at $a = 0.5$ as small scales dominate. At late times ($a = 2$), the effect of the plane wave makes the mass function of T_05L, T_10L and T_20L similar.

Not surprisingly, the presence of large-scale power leads to the formation of more massive haloes. However it does not seem to enhance the total mass in collapsed haloes.

4 DISCUSSION

In this paper we studied the effect of substructure on collapse of a plane wave. The key conclusions of the present study of the role of substructure are as follows.

(i) The pancake formed due to collapse of the plane wave is thinner if the infalling material is formed of collapsed substructure.

(ii) We show that collisions between clumps lead to enhancement of velocities transverse to the direction of large-scale collapse.

(iii) We show that in simulations with substructure where collisions are suppressed, pancakes are not thinner.

(iv) Thus collision-induced enhancement of motions transverse to the collapsing plane wave takes away kinetic energy from the direction of infall and leads to thinner pancakes.

(v) The presence of large-scale power shifts the mass function towards larger masses. There is, however, no change in the total mass in collapsed haloes.

The points outlined above essentially relate to coupling of density fluctuations at well separated scales. Each of these points refers to a measurable effect of such a coupling. The nature of large-scale fluctuation, a single plane wave, does not allow us to estimate the effect in terms of statistical indicators like the power spectrum. We plan to study these aspects with larger (256^3) simulations where the large-scale collapse will also be generic. Large, high-resolution studies are needed as 128^3 simulations with particle mesh code

have not shown any large effect in the power spectrum at late times (Bagla & Padmanabhan 1997a).

Another important point to consider is that we have considered two well-separated scales for fluctuations and there is no infall once fluctuations at the larger scales collapse. Numerical experiments that can shed light on the effects of this feature are also required to improve our understanding of the issues.

We also compared the collapse of a plane wave in an N-body with the collapse in the adhesion model with a finite effective viscosity. We found that:

(i) the adhesion model predicts the variation of density very well with a constant effective viscosity in regions with a given number of streams;

(ii) regions with a given number of streams coincide with the adhesion model with the same value of effective viscosity at all epochs.

ACKNOWLEDGMENTS

JSB thanks R. Nityananda, T. Padmanabhan and K. Subramanian for useful discussions and suggestions. JSB also thanks Varun Sahni and Uriel Frisch for a useful discussion on related issues. Numerical experiments for this study were carried out at the cluster computing facility in the Harish-Chandra Research Institute (http://cluster.mri.ernet.in). This research has made use of NASA's Astrophysics Data System.

REFERENCES

Bagla J. S., 2002, JA&A, 23, 185
Bagla J. S., 2005, Current Science, 88, 1088
Bagla J. S., Padmanabhan T., 1997a, MNRAS, 286, 1023
Bagla J. S., Padmanabhan T., 1997b, Pramana, 49, 161
Bagla J. S., Padmanabhan T., 1994, MNRAS, 266, 227
Bagla J. S., Ray S., 2003, New Astron., 8, 665
Bernardeau F., Colombi S., Gaztanaga E., Scoccimarro R., 2002, Phys. Rep., 367, 1
Bertschinger E., 1998, ARA&A, 36, 599
Bond J. R., Myers S. T., 1996a, ApJS, 103, 1
Bond J. R., Myers S. T., 1996b, ApJS, 103, 41
Bond J. R., Myers S. T., 1996c, ApJS, 103, 63
Brainerd T. G., Scherrer R. J., Villumsen J. V., 1993, ApJ, 418, 570
Couchman H. M. P., Peebles P. J. E., 1998, ApJ, 497, 499
Engineer S., Kanekar N., Padmanabhan T., 2000, MNRAS, 314, 279
Evrard A. E., Crone M. M., 1992, ApJ, 394, L1
Gurbatov S. N., Saichev A. I., Shandarin S. F., 1989, MNRAS, 236, 385
Hamilton A. J. S., Matthews A., Kumar P., Lu Edward, 1991, ApJ, 374, L1
Hui L., Bertschinger E., 1996, ApJ, 471, 1
Jain B., Mo H. J., White S. D. M., 1995, MNRAS, 276, L25
Klypin A. A., Melott A. L., 1992, ApJ, 399, 397
Little B., Weinberg D. H., Park C., 1991, MNRAS, 253, 295
Lynden-Bell D., 1967, MNRAS, 136, 101
Ma C.-P., Bertschinger E., 2004, ApJ, 612, 28
Ma C.-P., Boylan-Kolchin M., 2004, Phys. Rev. Lett., 93, 021301
Matarrese S., Lucchin F., Moscardini L., Saez D., 1992, MNRAS, 259, 437
Melott A. L., Shandarin S. F., Splinter R. J., Suto Y., 1997, ApJ, 479, L79
Monaco P., Theuns T., Taffoni G., Governato F., Quinn T., Stadel J., 2002a, ApJ, 564, 8
Monaco P., Theuns T., Taffoni G., 2002b, MNRAS, 331, 587
Nityananda R., Padmanabhan T., 1994, MNRAS, 271, 976
Padmanabhan T., 1996, MNRAS, 278, L29
Padmanabhan T., 2002, Theoretical Astrophysics: Galaxies and Cosmology, Vol. 3. Cambridge Univ. Press, Cambridge
Peacock J. A., 1998, Cosmological Physics. Cambridge Univ. Press, Cambridge
Peacock J. A., Dodds S. J., 1996, MNRAS, 280, 19
Peebles P. J. E., 1974, A&A, 32, 391
Peebles P. J. E., 1980, Large Scale Structure of the Universe. Princeton Univ. Press, Princeton
Peebles P. J. E., 1985, ApJ, 297, 350
Peebles P. J. E., 1990, ApJ, 365, 27
Ray S., Bagla J. S., 2004, astro-ph/0405220
Sahni V., Coles P., 1995, Phys. Rep., 262, 1
Shandarin S. F., Zeldovich Y. B., 1989, Rev. Mod. Phys, 61, 185
Smith R. E. et al., 2003, MNRAS, 341, 1311
Splinter R. J., Melott A. L., Shandarin S. F., Suto Y., 1998, ApJ, 497, 38
Springel V., Yoshida N., White S. D. M., 2001, New Astron., 6, 79
Subramanian K., 2000, ApJ, 538, 517
Taffoni G., Monaco P., Theuns T., 2002, MNRAS, 333, 623
Valinia A., Shapiro P. R., Martel H., Vishniac E. T., 1997, ApJ, 479, 46
Weinberg M. D., 2001, MNRAS, 328, 311
Weinberg D. H., Gunn J. E., 1990, MNRAS, 247, 260
Zel'dovich Ya. B., 1970, A&A, 5, 84

This paper has been typeset from a TEX/LATEX file prepared by the author.